BIOCHEMISTRY
including biophysical chemistry & molecular biology
Article

Biochemistry **2009,** *48,* 8985–8993 8985
DOI: 10.1021/bi900833f

The Role of Arginine-127 at the Proximal NO-Binding Site in Determining the Electronic Structure and Function of 5-Coordinate NO-Heme in Cytochrome *c′* of *Rhodobacter sphaeroides*[†]

Byunghoon Lee,[‡] Oleg M. Usov,[‡] Vladimir M. Grigoryants,[‡] William K. Myers,[‡] James P. Shapleigh,[§] and Charles P. Scholes*[,‡]

[‡]*Department of Chemistry, Center for Biochemistry and Biophysics, University at Albany, State University of New York, Albany, New York 12222, and* [§]*Department of Microbiology, Wing Hall, Cornell University, Ithaca, New York 14853*

Received May 14, 2009; Revised Manuscript Received August 14, 2009

ABSTRACT: Cytochrome *c′* is a heme protein from a denitrifying variant of *Rhodobacter sphaeroides* which may serve to store and transport metabolic NO while protecting against NO toxicity. Its heme site bears resemblance through its 5-coordinate NO-binding capability to the regulatory site in soluble guanylate cyclase. A conserved arginine (Arg-127) abuts the 5-coordinate NO-heme binding site, and the alanine mutant R127A provided insight into the role of the Arg-127 in establishing the electronic structure of the heme-NO complex and in modifying the heme-centered redox potential and NO-binding affinity. By comparison to R127A, the wild-type Arg-127 was determined to increase the heme redox potential, diminish the NO-binding affinity, perturb and diminish the ^{14}NO hyperfine coupling determined by ENDOR (electron nuclear double resonance), and increase the maximal electronic *g*-value. The larger isotropic NO hyperfine and the smaller maximal *g*-value of the R127A mutant together predicted that the Fe−N−O bond angle in the mutant is larger than that of the Arg-127-containing wild-type protein. Deuterium ENDOR provided evidence for exchangeable H/D consistent with hydrogen bonding of Arg-127, but not Ala-127, to the O of the NO. Proton ENDOR features previously assigned to Phe-14 on the distal side of the heme were unperturbed by the proximal side R127A mutation, implying the localized nature of that mutational perturbation at the proximal, NO-binding side of the heme. From this work two functions of positively charged Arg-127 emerged: the first was to maintain the K_D of the cytochrome *c′* in the 1 μM range, and the second was to provide a redox potential that enhances the stability of the ferrous heme.

Cytochrome *c′* (Cyt *c′*) is a crystallographically characterized 5-coordinate ferrous NO-heme protein where an exogenous NO ligand replaces the proximal histidine found in the ferric protein (*1*−*3*). The Cyt *c′* that we study is expressed from the denitrifying bacteria *Rhodobacter sphaeroides* 2.4.3 (*4*−*6*), which uses NO as a metabolic intermediate. The critical amino acids near the heme in Cyt *c′* that can modulate the unusual 5-coordinate NO binding are schematically shown in Figure 1. On the proximal side of the heme, where the NO binds, there is a positively charged Arg (Arg-127 in *R. sphaeroides*) which is thought to hydrogen bond to the NO and modify its dissociation constant. On the opposite (distal) side is a large hydrophobic group which occludes NO binding. In *R. sphaeroides* this occluding group is Phe-14. Theoretical calculations aimed at understanding the propensity of NO to bind in a 5-coordinate fashion have probed the effect of an *in silico* Arg to Gly mutation (*7*); our *in vitro* study uses an Arg-127 to Ala-127 mutation to probe the structure/function relationship of Arg-127 in establishing the electronic structure of the heme-NO complex and the NO-binding and redox functions of the heme.

We have previously investigated the NO and its binding site in wild-type protein by electron nuclear double resonance (ENDOR) (*6*, *8*). ENDOR provided a direct hyperfine probe of the unpaired electron spin density on the nitrogen of NO, indicating that the electron spin on NO did not simply reside in a π^* orbital having only 2p character but had 2s character similar to but slightly smaller in magnitude than that of a 5-coordinate NO-heme crystalline model (*9*). We found strong proton hyperfine evidence for the nearest protons of the Phe-14 group which occludes ligand binding on the distal side. An exchangeable deuteron ENDOR spectrum was consistent in its deuteron hyperfine couplings with the hyperfine interaction of H/D hydrogen bonded to O of NO. Without change in the Arg-127 group to a non-hydrogen bonding group, it could not be established that these deuterons were the ones that would exchange with the protons of Arg-127. There is a proximal His-123 which ligates to the heme in the ferric Cyt *c′*, and so an additional reason for making the R127A[1] mutation was to determine the necessity of Arg-127 in facilitating the replacement of His-123 when NO binds proximally to the heme and replaces His-123.

To perform these studies, we used an expression system requiring growth in *R. sphaeroides* itself but with mutagenesis

[†]This work supported by NIH Grant EB00326929 to C.P.S. and DOE Grant 95ER20206 to J.P.S.

*Corresponding author. Telephone: 518-442-4551. Fax: 518-442-3462. E-mail: cps14@albany.edu.

[1]Abbreviations: RF, radio frequency; EPR, electron paramagnetic resonance; mW, milliwatts; μW, microwatts; G, gauss; ν_{EPR}, EPR frequency; ν_{ENDOR}, ENDOR frequency; ν^P, proton nuclear Zeeman frequency; ν^D, deuteron nuclear Zeeman frequency; $^{14}\nu$, ^{14}N nuclear Zeeman frequency; R127A, mutant form of *R. sphaeroides* Cyt *c′* in which Arg-127 has been mutated to Ala-127; PMS, phenazine methosulfate; NADH, nicotinamide adenine dinucleotide.

Published on Web 08/17/2009

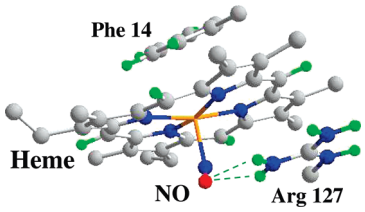

FIGURE 1: A scheme of the locale of the heme group in Cyt *c′* showing the NO, the arginine near the NO (Arg-127 in *R. sphaeroides*), and the occluding distal Phe-14. Since no crystal structure of NO-Cyt *c′* is available from *R. sphaeroides*, this composite graphic was created from the heme, NO, and arginine coordinates of the NO-Cyt *c′* of *A. xylosoxidans* (1E85) and the Phe-14 and heme coordinates of ferric Cyt *c′* of *R. sphaeroides* (1GQA) by application of Swiss PdB Viewer software. The numbering system is that of *R. sphaeroides*. There were two crystallographically resolved orientations of the NO, and the closer one to Arg-127 is shown. The putative positions of protons were provided by Swiss PdB Viewer software. Plausible hydrogen bonds from the nearest guanidinium protons of Arg-127 to the O of NO are schematically indicated.

performed on a plasmid propagated through *Escherichia coli*. A different heterologous *E. coli* expression system for Cyt *c′* of *Alcaligenes xylosoxidans* (*A. xylosoxidans*) has been reported (*10*) which additionally required a plasmid developed by L. Thöny-Meyer (*11*) that carried a suite of critical genes required for the maturation of *c′* cytochromes. UV−vis spectroscopy in this previous study (*10*) showed a minor difference in the pH dependence of the ferric spin state between the wild type and the Arg-to-Ala mutant that corresponded to R127A in *R. sphaeroides*. The presence of the naturally occurring Arg group, or a positively charged lysine, was found to enhance the transient presence of a 6-coordinate NO-heme-His species (*10*).

MATERIALS AND METHODS

Materials. The expression and purification of Cyt *c′* from the denitrifying *R. sphaeroides* 2.4.3 are summarized by Choi et al. (*4*) and Usov et al. (*6*). The approach applicable to the non-His-tagged version of Cyt *c′* used here is given in the Supporting Information of Usov et al. (*6*). A method for expression and purification of the present wild-type and mutant Cyts *c′* is given here in the present Supporting Information, and the explicit mutagenesis protocol for making the R127A mutant of Cyt *c′* from the denitrifying *R. sphaeroides* 2.4.3 is provided. The wild-type and mutant Cyt *c′* proteins were obtained through an overexpression system based on the overexpression plasmid pRK415 expressed in a Cyt *c′*-knockout variant of *R. sphaeroides* 2.4.3 (*4*). Expression of Cyt *c′* in *R. sphaeroides* required a more elaborate method of mutating the Cyt *c′* gene, first cloning and amplifying it in *E. coli* but then conjugating it in the broad host range plasmid pRK415 so it could be reintroduced back into *R. sphaeroides*. The expression construct included *cycP*, which codes for Cyt *c′* protein, and a strong, constitutive promoter, *rrnB*, to enhance expression levels. *cycP* was cloned downstream of *rrnB* which had been previously introduced into pRK415 (*4*).

For preparation of samples for EPR and ENDOR spectroscopy NADH (Sigma) was used as a reductant and PMS (Sigma) as a redox mediator. ^{14}NO of 98.5% chemical purity was purchased from Sigma-Aldrich. The NO gas at 1 atm of pressure was scrubbed through concentrated pH 7 phosphate buffer and anaerobically withdrawn into gastight Hamilton syringes that had been preflushed with argon. Samples of wild-type and mutant protein for EPR/ENDOR were prepared anaerobically at an approximate 1 mM protein concentration in pH 7.0, 0.05 M phosphate buffer under scrubbed NO gas, where the NO partial pressure above the samples in the anaerobic reaction vial was on the order of an atmosphere to ensure NO saturation of the heme sites. These samples of approximately 50 μL volume contained 50% glycerol by volume to favor glass formation (*8*). Deuteration of exchangeable protons was performed according to methods described in Usov et al. (*8*).

Spectroscopic Methods. Optical spectra were recorded with a Shimadzu dual beam spectrophotometer (slit width = 1.0 nm). The spectrometer was also used in a single beam mode to collect redox titration data. X-band EPR (9.45 GHz) was carried out at 77 K with a liquid nitrogen quartz tail insertion dewar. Q-band (34.1 GHz) ENDOR and EPR measurements were performed under dispersion (χ'), rapid passage, field-modulated conditions with a cryogenically tunable TE011 Q-band resonator (*12*) at 2 K as previously reported (*6*, *8*, *13*). In doing ENDOR, we monitored the radio frequency- (RF-) induced change in the rapid-passage, 100 kHz field-modulated dispersion EPR signal as we swept the frequency of the RF field. Through previous experience we have determined that strongly coupled protons (coupling $\geq$4 MHz) and nitrogens are best resolved with a higher field modulation $\geq$1 Gauss ptp (peak-to-peak) while weakly coupled nuclei, notably deuterons here, are best resolved with a smaller field modulation $\leq$0.5 Gauss ptp.

Redox Potential Measurements. Potentials were measured in a 50 mM pH 7.05 phosphate buffer by an Ingold-Metler/Toledo combined redox electrode (Pt4805-S7) after methods of Reinhammar (*14*). The electrode was calibrated with reference to the ferri/ferrocyanide redox couple under the same buffer conditions (*15*). Fourteen millimolar NADH and 1 mM ferricyanide were respectively the reductant and oxidant, and 10 μM PMS was the redox mediator. Under an argon atmosphere at 23 °C with stirring, redox titrations were performed in a septum-stoppered optical cell. Each aliquot for titration was injected via Hamilton gastight syringe, and optical absorbances were corrected for dilution. The redox-sensitive optical absorbances at 494 and 546 nm were monitored spectrophotometrically, and entire optical traces from 700 to 400 nm were taken at each potential following addition of oxidant or of reductant and a wait of at least 10 min to achieve redox equilibrium. (A_{494} is largest when the protein is oxidized; A_{546} is largest when the protein is reduced.) Every redox titration was carried out in both a reductive sense by adding NADH and an oxidative sense by adding ferricyanide. The ratio of oxidized to reduced Cyt *c′*, [(ox)/(red)], was obtained from the average value of the ratio of absorbances, taken at 494 nm as $(A_{494} - A_{red})/(A_{ox} - A_{494})$ and taken at 546 nm $(A_{546} - A_{red})/(A_{ox} - A_{546})$. A_{ox} was the absorbance when the protein was completely oxidized, and A_{red} was the absorbance when the protein was completely reduced.

NO-Binding Titrations. Prior to NO binding, reduction of 10 μM Cyt *c′* to its ferrous form was done by adding a 5-fold molar excess of sodium dithionite in an argon-purged solution to the protein also in an argon-purged, septum-stoppered cuvette. Buffer saturated by 1 atm of NO was used as the NO solution for titration, and this solution was anaerobically withdrawn from an anaerobic solution of buffer that had been equilibrated with 1 atm of scrubbed NO. During NO titrations microliter aliquots of this stock 2 mM NO solution were transferred into the

septum-stoppered optical cuvette that contained reduced protein, and allowed to equilibrate for 10 mins at 23 °C. The concentration of free NO in solution was determined by first subtracting the number of moles of heme-bound NO as determined by optical absorbance (430.6 nm) from the molar amount of added NO and subsequently allowing the resultant free NO to partition, according to Henry's law, as NO gas in the known head space of the cuvette and as free NO in solution. (The NO concentration in equilibrium with 1 atm of pressure of NO gas at room temperature is ≈2 mM in NO by application of the Henry's law constant of 5×10^2 (L atm/mol). From the *CRC Handbook of Chemistry and Physics*, 1981.)

ENDOR Theory: Protons/Deuterons. The frequencies of proton or deuteron ENDOR features, ν_{ENDOR}, center to first order at the respective free proton or free deuteron nuclear Zeeman frequency, ν^P or ν^D, where at a field of 1.200 T ν^P = 51.09 MHz and ν^D = 7.84 MHz. Taking A as the hyperfine coupling, one finds the frequencies, ν_{ENDOR}, are split away from the nuclear Zeeman frequency by $\pm^1/_2A$ for protons coupled to the electron spin $^1/_2$ doublet. Proton ENDOR frequencies, occurring as "+" or as "−" Zeeman branches, are (*16*)

$$^P\nu^{\pm}{}_{ENDOR} = |\nu^P \pm {}^PA/2| \quad (1)$$

With the neglect of small quadrupolar terms, a similar expression holds for deuterons:

$$^D\nu^{\pm}{}_{ENDOR} = |\nu^D \pm {}^DA/2| \quad (2)$$

First-order expressions hold here because $\nu^P \gg {}^PA/2$ and $\nu^D \gg {}^DA/2$.

The dipolar coupling to spin localized on the iron is explained by point dipolar coupling A_{PTdip} (*8*), which is

$$A_{PTdip}(3\cos^2\omega - 1) = (f_{Fe}g_{eff}g_n\beta_e\beta_n/hR^3)(3\cos^2\omega - 1) \quad (3)$$

$$A_{PTdip} = (f_{Fe}g_{eff}g_n\beta_e\beta_n/hR^3) = (39.5f_{Fe}g_{eff}/R^3) \quad (MHz)$$

where f_{Fe} is the fraction of an unpaired electron on the iron ($f_{Fe} \sim 0.9$ here), g_{eff} is the electronic g-value where the dipolar interaction is measured, g_n is the nuclear g-value (= 5.585 for a proton), **R** is the metal-to-proton vector, R is the iron−proton distance, and ω is the angle between the vector **R** and the external magnetic field.

Nitrogen ENDOR Frequencies and Hyperfine Analyses. The first-order expressions for spin 1 ^{14}N ENDOR frequencies for heme, histidine, and NO are

$$^{14}\nu^+\text{ENDOR} = |^{14}A/2 \pm 3/2P + {}^{14}\nu| \text{ and } {}^{14}\nu^-\text{ENDOR} = |^{14}A/2 \pm 3/2P - {}^{14}\nu| \quad (4)$$

where ^{14}A is the hyperfine coupling, P is the quadrupolar coupling, and $^{14}\nu$ (= 3.75 MHz at 1.218 T) is the ^{14}N nuclear Zeeman frequency. (If quadrupolar splitting is resolved, the quadrupolar splitting will be $3|P|$.) For ^{14}N nitrogen, as opposed to protons, the hyperfine term, $^{14}A/2$, rather than the nuclear Zeeman term, is the dominant term.

RESULTS

Spectroscopic Results. (*A*) *UV−Vis*. The optical spectra for the ferric, ferrous, ferrous-CO, and ferrous-NO derivatives of the wild type and the mutant R127A of *R. sphaeroides* Cyt *c′* are given in Figure 2, and peak wavelengths and extinction coefficients are given in Table 1. The peak wavelengths of R127A and wild type were within 1 nm of each other. These spectra are similar to those of the corresponding derivatives of Cyts *c′* from other species (*17*), and the CO-bound form indicated 6-coordination (CO-heme-His) while the NO-bound form indicated 5-coordination (NO-heme). There was a shoulder at 414 nm in the NO-ligated wild-type Cyt *c′* spectrum (see Figure 2S, Supporting Information) which may imply a small contribution from 6-coordinate NO-heme-His.

(*B*) *EPR*. A comparison of X-band EPR spectra from the NO derivatives of R127A and wild-type Cyt *c′* is shown in Figure 3. Both complexes have a characteristic three-line ^{14}NO hyperfine pattern centered at a g-value near 2.008; such features, lacking histidine nitrogen hyperfine splitting, indicate 5-coordinate ^{14}NO-heme. The EPR-resolved hyperfine coupling is slightly larger for the mutant at 17.0 ± 1.0 G (= 48.1 ± 2.8 MHz) than for the wild type at 16.0 ± 1.0 G (= 45.3 ± 2.8 MHz). Since 6-coordinate NO-heme-His complexes have a minimal g-value less than 2.00, lack of any such features below g = 2.00 is evidence against 6-coordination and is a strong indication that Arg-127 is not obligate for NO 5-coordination. There was difference between the NO-ligated R127A and wild-type Cyt *c′* in the

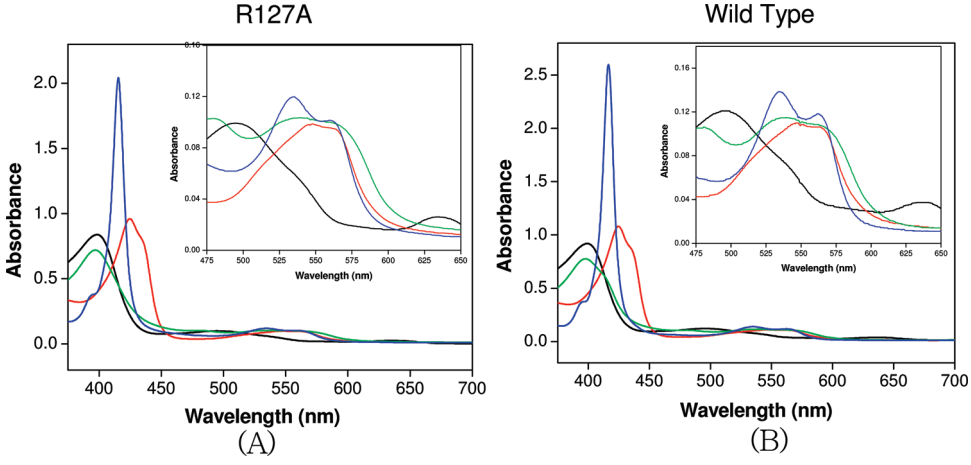

FIGURE 2: UV−vis absorption spectra of (A) mutant (R127A) and (B) wild- type *R. sphaeroides* Cyts *c′*. Heme concentration is 10 μM in 100 mM phosphate buffer, pH 7. The black spectrum is ferric, the red spectrum is ferrous, the green spectrum is the NO-bound ferrous, and the blue spectrum is the CO-bound ferrous.

Table 1: Electronic Absorption Maxima (nm) and Extinction Coefficients[a] (L mmol^{-1} cm^{-1})

derivative	Soret	visible α−β	
	Wild Type		
ferric	399 (92)	495 (12)	635 (3.7)
ferrous	424.5 (108)	547 (11)	
NO ferrous	397.5 (77), 414 sh (69)	540 (12)	
CO ferrous	416.6 (255)	534.5 (14)	560.5 (11)
	Mutant (R127A)		
ferric	398.5 (84)	495 (10)	635 (2.8)
ferrous	424.5 (96)	547 (10)	
NO ferrous	397 (66)	540 (10)	
CO ferrous	415.5 (205)	535 (12)	560 (10)

[a]The underlying heme concentrations needed to estimate the extinction coefficients were obtained by a pyridine hemochrome assay (*18*).

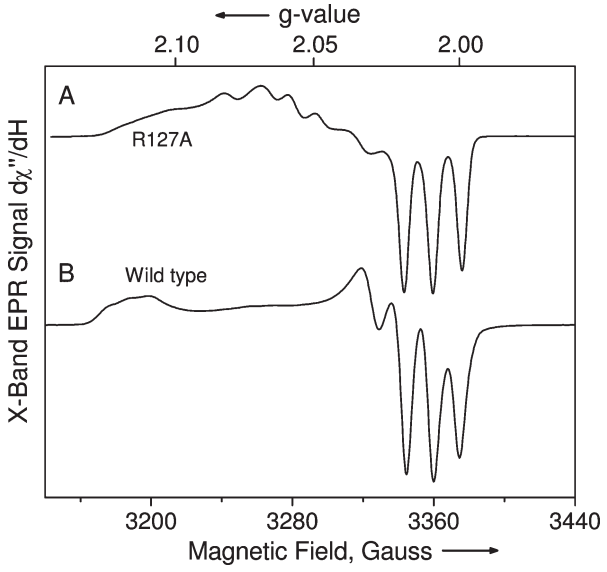

FIGURE 3: X-band EPR spectra of the ferrous ^{14}NO derivatives of (A) the R127A mutant and (B) wild-type Cyt *c′*. The spectra were recorded at T = 77 K, 3 G field modulation, 100 s of signal averaging, 2 mW microwave power, and EPR frequency ν_{EPR} = 9.446 GHz.

higher *g*-value, lower field region near g = 2.10. The maximum *g*-value (2.12) for wild-type NO-ligated Cyt *c′* was greater than the maximal *g*-value(s) associated with the mutant NO complex. The EPR spectrum of the R127A mutant showed at least two species having differing values of g_{max}; the majority species had a maximal *g*-value of about 2.075; there was a minority species with g_{max} of about 2.11. The majority species also showed evidence in the region from g = 2.05−2.08 for hyperfine splittings comparable to those observed near g = 2.01. The overall EPR spectrum of the R127A bore resemblance to NO-ligated soluble guanylate cyclase in the absence of activator (see Figure 3 of Derbyshire et al. (*19*)) where *g*-strain broadening was invoked to explain the breadth of the g_{max} region (*19*). Q-band EPR spectra, which are more sensitive to *g*-value differences (Figure 3S, Supporting Information), also indicated that the majority species from the NO-bound R127A had a g_{max} value of about 2.075, while there was a minority species with its g_{max} slightly less than that of wild-type Cyt *c′*. For completeness here, we additionally

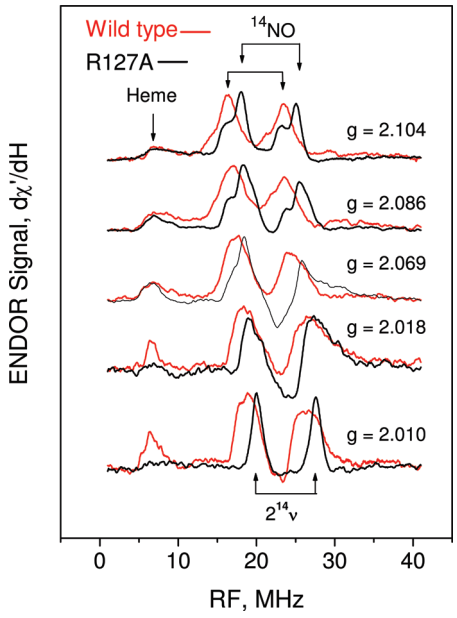

FIGURE 4: Nitrogen ENDOR spectra of the ^{14}NO-ligated R127A mutant (black) and wild-type Cyt *c′* (red) at the following magnetic fields: 1.158 T (g = 2.104), 1.168 T (g = 2.086), 1.178 T (g = 2.069), 1.208 T (g = 2.018), and 1.212 T (g = 2.010). Arrows indicate ^{14}N nuclear Zeeman splitting of 2 $^{14}\nu$. Conditions were adiabatic rapid passage, T = 2 K, microwave power = 0.22 nW, 100 kHz field modulation = 5 G ptp, system time constant = 160 ms, RF power ≈ 20 W, radio frequency sweep rate = 2 MHz/s, overall signal averaging time = 400 s, and ν_{EPR} = 34.10 GHz. RF power was pulsed with a 100/900 μs duty cycle.

Table 2: ^{14}NO Hyperfine Couplings of R127A and Wild-Type Cyt *c′*

complex	coupling (MHz)	method	*g*-value	ref
R127A	$^{14}A_{min}$ = 43.1 ± 0.6	ENDOR	2.104	this work
	$\|P\|$ = 0.62 ± 0.10		2.104	
	$^{14}A_{max}$ = 47.6 ± 0.6		2.010	
	$^{14}A_{max}$ = 48.1 ± 2.8	EPR	~2.010	
wild type	$^{14}A_{min}$ = 35.7 ± 0.6	ENDOR	2.122	*8*
	$\|P\|$ = 0.65 ± 0.10		2.122	
	$^{14}A_{max}$ = 43.7 ± 0.6		2.010	
	$^{14}A_{max}$ = 45.3 ± 2.8	EPR	~2.010	

point out that the ferric derivative of wild-type Cyt *c′* has a characteristic mixed-spin sextet−quartet character (*6*); EPR and ^{14}N-histidine ENDOR showed very little difference between the ferric derivatives of R127A and the wild-type Cyt *c′* (see Supporting Information, Figures 4S and 5S).

(*C*) *^{14}NO ENDOR*. The comparison of Figure 4 shows that the ^{14}NO hyperfine coupling of the NO-ligated R127A mutant was consistently larger than that of the wild-type NO-ligated Cyt *c′*. The ^{14}N NO hyperfine coupling of NO R127A increased from 43.1 to 47.6 MHz in the *g*-value range of 2.104 to 2.010 while that of wild type increased from 35.7 to 43.7 MHz. Both $^{14}\nu^{+}_{ENDOR}$ and $^{14}\nu^{-}_{ENDOR}$ features were observed, and the expected Zeeman splitting of 2($^{14}\nu$) was resolved. The ^{14}NO quadrupole coupling, $|P|$, which is apparent at the high *g*-value, was the same within experimental error for the mutant and the wild-type proteins. As indicated in Table 2, the average (isotropic) value of hyperfine coupling for ^{14}NO is larger for the mutant than for wild type, while the anisotropic difference between couplings measured at g_{max} and at g_{min} is less.

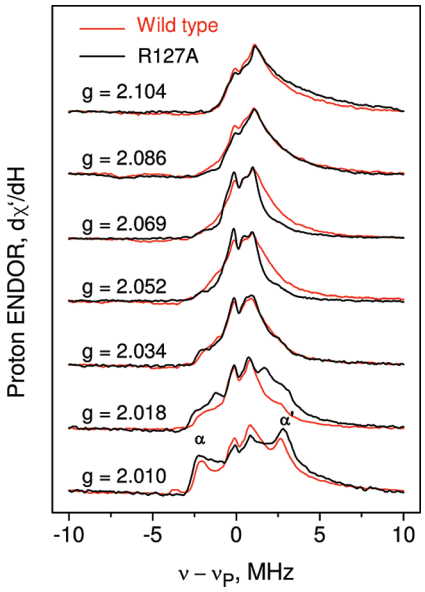

FIGURE 5: A comparison of the strongly coupled proton ENDOR spectra of the ^{14}NO-bound ferrous forms of the R127A mutant (black) and wild type (red) at the *g*-values indicated. Protons α and α′ were previously assigned as the nearest protons of Phe-14. Data were obtained under the following conditions: adiabatic rapid passage, T = 2 K, microwave power = 0.22 nW, 100 kHz field modulation = 2 G ptp, system time constant = 160 ms, RF power ≈ 20 W, radio frequency sweep rate = 2 MHz/s, overall signal averaging time = 400 s, and ν_{EPR} = 34.10 GHz. RF power was pulsed with a 100/900 μs duty cycle.

(*D*) *Proton and Deuterium ENDOR*. There was similarity of the strongly coupled proton features of NO-ligated wild type and R127A, as shown in Figure 5. A minor difference was observed near g_{min} = 2.018 in the resolution of protons (α, α′) previously assigned as the nearest protons of Phe-14 (*8*), implying at most a slight difference in the orientation of the minimal *g*-tensors of NO-ligated R127A and wild-type Cyt *c*′ with respect to the coordinates of Phe-14.

As previously noted, proton ENDOR failed to reveal definitive evidence for exchangeable protons (*8*) because nonexchangeable and exchangeable proton features were highly overlapped. Exchangeable deuteron ENDOR spectra revealed evidence for those deuterium/protons that would exchange, and in the work reported here a significant difference between wild-type Cyt *c*′ and the R127A mutant emerged, as shown in Figure 6. A broad feature with deuterium hyperfine coupling of 0.37 ± 0.05 MHz was observed for the wild-type protein, which has a Arg-127 side chain capable of hydrogen bonding to NO, and no such feature was observed from the R127A mutant whose Ala-127 side chain lacked hydrogen bonding capability. (A deuterium coupling of 0.37 MHz corresponds to a proton hyperfine coupling of 2.4 MHz; proton features with such couplings were overlaid and obscured by nonexchangeable protons.) Details of the distance to these deuterons and the possibility of their being involved with an H-bond between the Arg-127 and the NO are discussed below. Both mutant and wild-type proteins showed a central deuterium ENDOR peak with an approximate 0.2 MHz width, which may reflect the existence of more distant exchangeable deuterons.

Redox Results: Midpoint Potentials. Redox titrations for the heme of wild-type and R127A Cyt *c*′ are shown in Figure 7 as a Nernst plot, where log([ox]/[red]) was plotted vs the electrode potential, *E*, for wild-type protein and the R127A mutant.

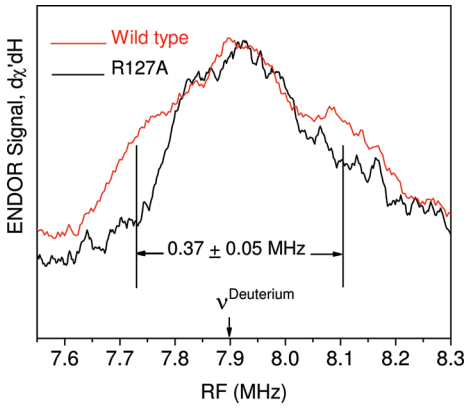

FIGURE 6: ENDOR spectra of D_2O-exchanged NO-Cyt *c*′ from R127A mutant (black) and wild type (red). These spectra were collected near the free deuterium ENDOR frequency of 7.9 MHz which occurs at the magnetic field of 1.208 T (g = 2.017). Experimental conditions were as follows: adiabatic rapid passage, T = 2 K, microwave power = 0.22 nW, 100 kHz field modulation = 0.15 G ptp, system time constant = 320 ms, RF power ≈ 20 W, RF sweep rate = 0.06 MHz/s, overall signal averaging time = 1200 s, and ν_{EPR} = 34.10 GHz. RF power was pulsed with a 100/900 μs duty cycle.

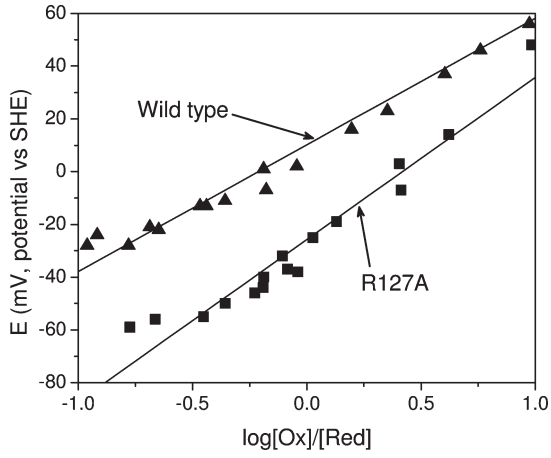

FIGURE 7: These traces show redox titrations in the form of Nernst plots for the heme group of Cyt *c*′ belonging to wild type (triangles) and R127A (squares). The midpoint potential for wild-type protein was +10 ± 3 mV. For R127A the midpoint potential was −24 ± 3 mV.

Following least-squares fitting of the Nernst equation to the experimental data, the midpoint reduction potential for the wild-type Cyt *c*′ was +10 ± 3 mV, whereas the midpoint reduction potential for R127A mutant was −24 ± 3 mV. The comparison of the midpoint potentials of the wild-type protein having positively charged Arg-127 near the heme and R127A having the Arg-127 replaced by an uncharged Ala demonstrates that the redox potential can be significantly modulated by a charged, nonliganding group near the heme.

NO Binding. An optically monitored NO titration of ferrous Cyt *c*′ provided a comparison of the NO-binding affinity of the heme group in wild type and R127A. As shown in Figure 8, the NO-induced change in the optical spectra of the Soret region was monitored as the NO concentration was increased. As indicated in the legend to that figure, NO bound to the heme of the R127A mutant at a lower NO concentration than for wild type. Detailed comparisons of the NO titration over a 350−700 nm range are presented in the Supporting Information, Figure 6S. There was

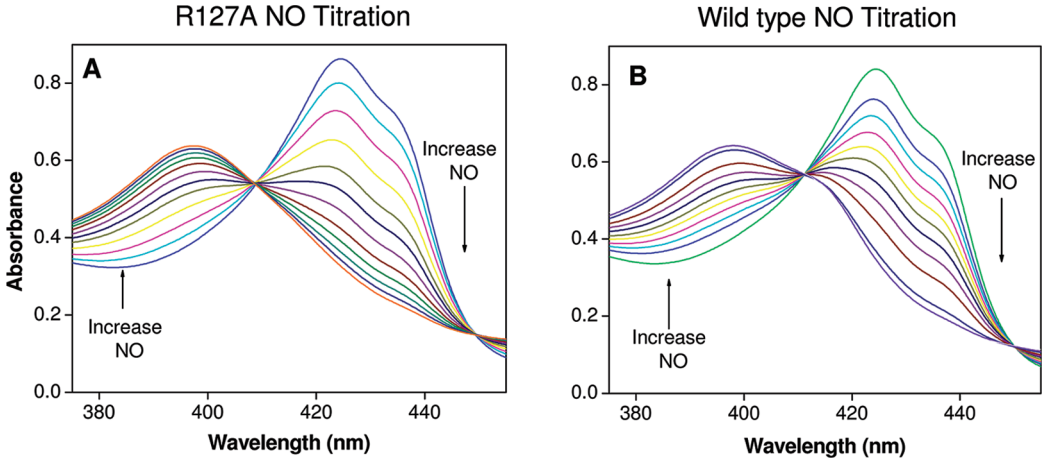

FIGURE 8: UV−vis titrations of (A) mutant Cyt *c*′ (R127A) and (B) ferrous wild-type Cyt *c*′, 10 μM protein in 100 mM phosphate buffer at pH 7.05. For (A), [NO] ($\times 10^{-7}$ M): 0.41 (blue), 0.80 (cyan), 1.13 (magenta), 1.44 (yellow), 1.77 (dark yellow), 2.24 (navy), 2.71 (purple), 3.22 (wine), 3.82 (olive), 4.45 (dark cyan), 5.12 (royal), and 5.82 (orange). For (B), [NO] ($\times 10^{-7}$ M): 1.33 (green), 2.74 (blue), 4.37 (cyan), 5.99 (magenta), 7.645 (yellow), 9.29 (dark yellow), 10.9 (navy), 12.5 (purple), 14.0 (wine), 19.3 (royal), and 23.0 (violet).

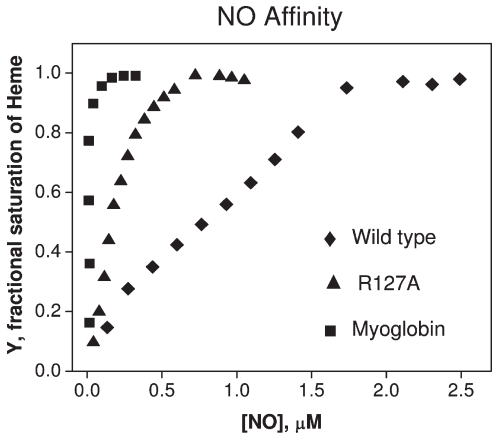

FIGURE 9: Fractional heme NO saturation levels (*Y*) are presented for ferrous myoglobin (squares), R127A (triangles), and wild-type Cyt *c*′ (diamonds) as a function of free NO concentration. The values of *Y* were determined from the NO-sensitive UV−vis spectra at 450.0 nm for myoglobin and at 430.6 nm for both Cyts *c*′. Free NO concentration was determined from the difference between added NO and protein-bound NO, as described in the Materials and Methods section.

evidence in the NO-binding plot of the wild-type protein for a shoulder at 414 nm, indicating a small contribution from 6-coordinate NO-heme-His, as pointed out in Figure 6S.

From the titration graphs of Figure 8 the fraction (*Y*) of heme groups with bound NO was calculated. The plot of *Y* vs NO concentration is provided in Figure 9 for wild-type Cyt *c*′, R127A, and ferrous myoglobin. Figure 9 definitively shows that the R127A mutant has a higher NO affinity by roughly a factor of 5, as measured by the respective NO concentrations at half-saturation ($Y = {}^1/_2$). The half-saturation concentrations of [NO] from Figure 9 were respectively 0.75 ± 0.05 and 0.15 ± 0.05 μM for wild type and R127A. The horse heart myoglobin, which is known to have a NO dissociation constant in the subnanomolar region (*20*), bound NO more strongly than did either Cyt *c*′. Although a detailed investigation of the cooperativity of NO binding to Cyt *c*′ is not the focus of this work, the plot of fraction NO bound (*Y*) divided by fraction of protein unbound ($1 - Y$), which would be linear if the binding were noncooperative, showed significant upward curvature (Figure 7S). This curvature implies positive cooperativity of NO binding, possibly, as previously proposed (*21*), because of the coupling of NO binding and protein dimerization.

DISCUSSION

Spectroscopic Information. (A) Spectroscopic Similarities of the R127A and Wild-Type Cyt c′. For ferric, ferrous, ferrous-CO, and ferrous-NO forms of R127A and wild-type Cyt *c*′ the UV−vis spectroscopic peak and shoulder wavelengths were essentially identical, and the extinction coefficients were within 10−20% of each other. Because the ferric, ferrous, and CO-ligated forms of these and homologous Cyts *c*′ have His ligation (His-123 here), the implication is that neither Arg-127 nor Ala-127 interacts sufficiently with His-123 to alter the porphyrin-centered optical spectra. The 5-coordinate NO-heme evidently does not interact sufficiently with Arg-127, versus Ala-127, to perturb its porphyrin-centered optical spectrum. The EPR spectra of the ferric R127A and wild-type Cyt *c*′ are virtually identical (Figure 4S) so that the R127A mutation does not perturb the metal 3d electronic levels and does not alter the quartet−sextet mixing of the ferric ground state, which was found by EPR to be about a 50:50 quartet:sextet admixture at pH 7.0 (*6*). The frequencies of heme and histidine nitrogen ENDOR from ferric R127A and wild-type Cyt *c*′ (Figure 5S), which are due to unpaired electron spin on the ligating His-123 and heme nitrogens, are also virtually identical, implying that the R127A mutation does not perturb the electronic spin distribution on the His-123 imidazole ring. All of these foregoing unchanged spectroscopic findings indicate that the R127A mutation causes no large proximal side conformational changes to the protein structure and imply that the histidine-ligated ferric heme is electronically unperturbed by the nearby R127A mutation.

For the 5-coordinate NO-heme of R127A and wild-type Cyt *c*′ the similarity of the strongly coupled nonexchangeable proton ENDOR (α, α′ in Figure 5) previously assigned to the nearest Phe-14 protons (*8*) is evidence that the overall conformation distal to the NO-binding site is also very similar in the wild type and R127A mutant. The proton hyperfine coupling of 4.7 MHz from the α, α′ proton features had previously been estimated to arise from dipolar coupling of spin on the iron to the nearest Phe-14 ring proton, 3.1 Å distant from the iron. The slight difference

in resolution of the α, α′ features in R127A is probably due to a slightly different orientation of the NO-heme *g*-tensor in R127A. The immediate conclusion is that the NO of the ferrous R127A mutant binds proximal to the heme in virtually the same location as the NO of wild-type Cyt *c*′ and that there is little perturbation at the distal side of the heme where Phe-14 occurs.

(*B*) *Spectroscopic Differences of R127A and Wild-Type Cyt c*′. ENDOR of ^{14}NO (Figure 4) and EPR of the 5-coordinate NO-heme (Figure 3) most notably did show differences between the R127A mutant and the wild-type Cyt *c*′. The ^{14}N ENDOR of NO showed that the average (isotropic) ^{14}N coupling of 45 MHz is larger for the R127A mutant than the average coupling of 40 MHz for the wild-type Cyt *c*′ which has retained Arg-127. On the other hand, the 4 MHz anisotropy in the ^{14}NO coupling of 4 MHz for the R127A mutant was smaller than the corresponding 8 MHz anisotropy for wild type. Isotropic coupling reflects 2s character of the unpaired electron spin, and the anisotropic coupling reflects 2p character of the electron spin. The explanation for these two findings is that the unpaired spin on the ^{14}N of NO in the R127A mutant has more isotropic 2s character but less anisotropic 2p character than does the wild type. Additionally, the maximum *g*-value, g_{max} in the range 2.08−2.11, for the R127A mutant was less than that of the wild type ($g_{max} \approx$ 2.12), especially so for the majority species having $g_{max} \approx 2.08$.

The larger contribution of 2s character of the ^{14}N of NO, the smaller contribution of 2p character, and a diminished value of g_{max} for the 5-coordinate NO-heme can be self-consistently explained. They results from an Fe−N−O bond angle that increases and tends closer to 180° in the R127A mutant than in the wild type. Such an angular change would alter the electronic character of the SOMO (singly occupied molecular orbital) containing the unpaired electron spin and the energy levels of the metal 3d orbitals and the n and π^* orbitals on the NO. In Scheme 1 used previously by Usov et al. (*8*), the SOMO had primarily (∼90%) d(z^2) character with the remainder of spin on the NO with n and π^*_x character (*8*, *9*, *22*). The SOMO accounts for hyperfine coupling to the NO and also, in combination with the energy levels of the d(*xz*) and d(*yz*) orbitals, for the *g*-values of 5-coordinate Fe-NO heme. As the Fe−N−O angle increases toward 180°, there will be more antibonding overlap of the d(z^2) orbital with the n orbital of the NO. This increased overlap will increase the amount of ^{14}NO 2s character in the SOMO and also raise the energy of the d(z^2) orbital through an antibonding interaction. As the Fe−N−O angle increases, there will be less overlap of the SOMO with the π^*_x orbital, thus diminishing the 2p character of the SOMO, and concomitantly diminishing the amount of back-bonding with d(z^2) and raising the energy of the SOMO. As the Fe−N−O angle increases, there will be an increased amount of back-bonding of the π^*_x orbital and the d(*xz*) orbital which will lower the d(*xz*) orbital energy. The difference in energy between the d(z^2)-containing SOMO and the d(*xz*) orbital will be increased as the Fe−N−O angle becomes larger. Spin−orbit coupling of the (dz^2) component of the SOMO to the energetically near d(*xz*) orbital accounts for $g_{max} > 2.00$. Specifically, after Hayes et al. (*9*), $g_{max} = g_o + 6\xi/\Delta_2$, where g_o is the free electron *g*-value, ξ is the iron spin−orbit coupling constant (335 cm^{-1}), and Δ_2 is the energy difference between the d(z^2) orbital and the d(*xz*) orbital. (In ref *9* this maximum *g*-value is called $g_{y'y'}$.) The upshot is an increase in the energy difference between the d(z^2) orbital and the d(*xz*) that causes g_{max} to decrease. Thus a mutation-induced increase in the Fe−N−O bond angle will cause an increase in ^{14}NO 2s spin density, a decrease in ^{14}NO 2p spin density, and a decrease in g_{max}. An increase in the Fe−N−O bond angle is predicted on comparison of wild type and R127A, although there is no direct formula for quantitatively predicting the Fe−N−O bond angle from *g*-values and NO hyperfine couplings (unlike the recent prediction of the Cu−N−O bond angle in Cu(I)NO systems from the minimal *g*-value (*23*)). For R127A, A_{iso} = 45 and g_{max} is in the range 2.08−2.11. For qualitative comparison, we note that in FeII(NO)-porphyrin crystals A_{iso} = 44 MHz and g_{max} = 2.11 as measured at 77 K (*9*), and in these crystals the Fe−N−O bond angle was ∼145° (*24*). Whereas, for wild-type *R. sphaeroides* NO-Cyt *c*′, there was a smaller A_{iso} = 40 MHz and a larger g_{max} = 2.12 (*8*), and as determined from the NO derivative of *A. xylosoxidans* Cyt *c*′ (*1*), the average Fe−N−O bond angle was 128°.

Scheme 1: Left: Energy levels, d-centered wave functions, and spin population of the low spin d^6 ferroheme. Center: Perturbed d-centered energy levels and wave functions after bonding to NO and bending of the Fe-N-O. The lowest energy orbital has primarily n character, the next six orbitals, including the SOMO, have primarily d character, and the two highest unfilled orbitals have primarily π^* character. These energy levels are schematic. Right: Important orbitals of the nitrosyl ligand. This scheme is taken from (*8*).

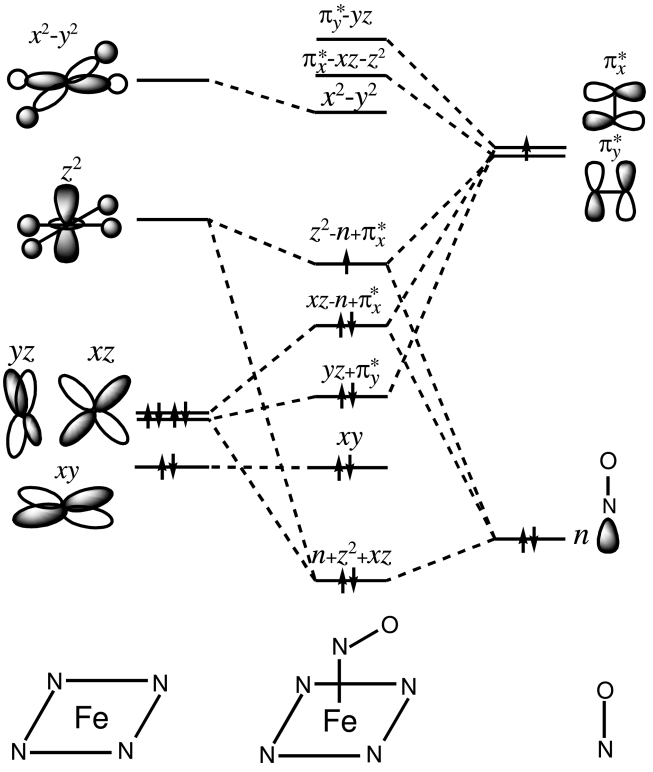

Exchangeable deuterium ENDOR spectra of the NO-Cyt *c*′ of R127A and wild type in Figure 6 were obtained to investigate the potential for hydrogen bonding between NO and protons on the guanidinium side chain of Arg-127. From the denoted outlying shoulders of Figure 6, a deuterium coupling of 0.37 MHz was estimated for the NO-Cyt *c*′ wild type, but this coupling was not observed for the R127A mutant. If the coupling to these deuterons were purely dipolar, then by use of eq 3, these deuterons would lie 3.2−4.0 Å distant from the iron, taking ω either as 0° or as 90° in eq 3. If they are bonding to O of the NO, it is possible that there is some Fermi contact interaction from direct covalent spin transfer to them. It may be that both dipolar coupling to spin on the iron and direct covalent spin transfer to

the deuterons account for their hyperfine coupling. In any case, the presence of these deuteron features is highly consistent with their origin on the hydrogen bonding guanidinium side chain of Arg-127. Their absence in R127A is highly consistent with the loss of Arg-127 and its replacement by a more distant and non-hydrogen bonding methyl side chain of Ala-127. The broad deuterium ENDOR feature near the free deuteron frequency is evidence that the ligand binding pocket may be open to more distant, exchangeable D_2O. The indication from exchangeable deuteron ENDOR is that Arg-127 abuts the NO so as to hydrogen bond to it. The R127A with smaller methyl group side chain may actually provide a less sterically perturbed NO environment. Furthermore, the existence of conformations of NO bound to R127A with different values of g_{max} may reflect the tendency found even in model porphyrin Fe-NO complexes of NO to show angular disorder about the Fe−N bond when less axially constrained (*24*).

Another difference between the R127A mutant and wild-type Cyt *c*′ is the small shoulder at 414 nm in the UV−vis from wild-type Cyt *c*′, a shoulder which implies existence of 6-coordinate NO-heme-His. We have previously noted by EPR the occasional existence of a small amount of 6-coordinate NO-heme-His from wild-type Cyt *c*′ (see p 5031 in Usov et al. (*8*)), where the 6-coordinate fraction was estimated by EPR to account for 10% of the total heme. Since a 6-coordinate NO-heme-His intermediate has been proposed as a transient predecessor to the final 5-coordinate NO-Cyt *c*′ species of *A. xylosoxidans* (*7*, *17*, *21*, *25*−*27*) , we have recently and successfully used rapid freeze-quench EPR to probe for early development of a 6-coordinate NO-heme-His intermediate from wild-type *R. sphaeroides* Cyt *c*′.[2]

Redox Potential. The redox potentials of Cyts *c*′ range from −10 to 150 mV (*28*). The liganding coordination at the heme center, the electrostatic interactions between the charge on heme and polar species within the protein and buffer, and the overall conformation of the Cyt *c*′ can in principle alter the redox potential. The positively charged side chain of Arg-127, which is lost in the R127A mutation, is 4−6 Å from the heme. Wild-type Cyt *c*′ with a midpoint potential of 10 mV has a 34 mV higher midpoint potential than R127A, indicating that the positively charged Arg-127 stabilizes the reduced form of the protein. The Ala-127 residue of R127A has no charge on its methyl side chain, and a conformational change due to the mutation is not evident from UV−vis, EPR, or ENDOR experiments. Thus the redox potential difference would seem to result from an electrostatically induced difference between charged Arg-127 and uncharged Ala-127. The redox potential change may also be mitigated by adjustment of neighboring waters and by the reorientation of the Arg-127 between ferric and ferrous forms (a movement which has been crystallographically observed in the *A. xylosoxidans* protein (*1*)).

NO Binding. Overall, NO binding to the ferrous heme center in Cyt *c*′ is affected by the large bulky distal substituent (Phe-14 here) which impedes access to the distal side, by the proximal His (His-123 here) which must be replaced by NO, and by the Arg-127 which abuts the NO-binding site (*7*). The [NO] concentration at half-saturation was 0.75 μM for wild-type Cyt *c*′ and 0.15 μM for R127A. By using a simple mass-action equilibrium, the dissociation constant, K_D can be estimated as the NO concentration at half-saturation, and the free energy of binding is then $RT\ln(K_D)$. For wild-type *R. sphaeroides* Cyt *c*′ the free energy of NO binding was estimated at −34.7 ± 0.4 kJ/mol, and for R127A the free energy of NO binding was −38.7 ± 0.4 kJ/mol. The free energy of NO binding is −39.3 kJ/mol for *Chromatium vinosum* Cyt *c*′ (*21*) and −65.9 kJ/mol per heme for myoglobin (*20*, *21*).[3]

The final 5-coordinate form of Cyt *c*′ with NO bound proximally and His-123 displaced is the stable form. A question which this work was intended to answer is whether for NO binding Arg-127 is relatively stabilizing due to its hydrogen bonding propensity or whether the combination of its steric bulk and hydrogen bonding offset each other and make Arg-127 destabilizing with respect to a smaller nonpolar Ala-127. An *in silico* mutation of Arg to Gly has been done (*7*), and the resultant theory indicated that the homologue of Arg-127 stabilized the 5-coordinate NO-bound form by 1.3 kcal/mol (= 5.5 kJ/mol) with respect to Gly. Our binding study indicated, through K_D values estimated from NO half-saturation, approximately 5-fold less NO affinity for the wild type as compared to the R127A mutant. That means that Arg-127 destabilizes the 5-coordinate NO-bound form by 4.0 ± 1.0 kJ/mol (or 0.9 kcal/mol). Thus the combination of its steric bulk and hydrogen bonding makes Arg-127 destabilizing for NO binding on comparison to a smaller nonpolar Ala-127.

CONCLUSIONS

The Cyt *c*′ mutant R127A was developed by site-directed mutagenesis and overexpressed in a Cyt *c*′ knockout strain of *R. sphaeroides* 2.4.3. The purpose of making this mutant was to probe the role of Arg-127, which closely abuts the proximal NO-to-heme binding site. Arg-127, with its positively charged, potentially hydrogen bonding guanidine, was compared to Ala-127 with its smaller methyl group. They were compared in their effect on the functional properties of redox potential and NO-binding affinity and in their effect on the intimate structural properties of NO and proton hyperfine couplings probed by ENDOR.

From a structural standpoint, it was determined that the Ala-127 mutation neither perturbed the local ferric heme electronic structure nor prevented the NO from binding to ferrous heme in 5-coordinate fashion. The R127A mutation on comparison to wild-type Cyt *c*′ led to an increased ^{14}NO isotropic hyperfine coupling and to a diminished value of g_{max}; these two findings taken together would predict, as indicated in the Discussion, a mutation-induced increase in the Fe−N−O bond angle to the R127A mutation. Deuterium ENDOR provided evidence of hydrogen bonding from the Arg-127 guanidinium group to O of NO, hydrogen bonding which was eliminated by the Ala-127 mutation. The steric bulk of the Arg-127, perhaps offset by its

[2]Rapid free-quench EPR work in progress shows that a 6-coordinate NO-heme-His complex of Cyt *c*′ arises within 10 ms of mixing reduced Cyt *c*′ and NO and continues to increase intensity for at least 38 ms. The ratio of 5-coordinate to 6-coordinate NO-Cyt *c*′ increases during that time.

[3]For a simple empirical comparison of NO affinity between wild-type Cyt *c*′ and R127A, we considered NO binding as described by a simple mass action equilibrium, $H\cdot NO \leftrightarrow H + NO$, where [H·NO] is the concentration of NO-bound heme, [H] is the concentration of unbound heme, and [NO] is the concentration of NO. Then $K_D = [H][NO]/[H\cdot NO]$ is the dissociation constant. When [H·NO] = [H] (i.e., $Y = {}^1/_2$), $K_D = [NO]_{1/2}$, where $[NO]_{1/2}$ is the NO concentration at half-saturation. The free energy of NO binding is then $RT\ln(K_D)$, where R is the gas constant and T is temperature, which was 296 K for our experiments.

hydrogen bonding capability, destabilized the binding of NO in comparison to the smaller Ala side chain replacement.

The wild-type Arg-127 of wild-type Cyt c' provided a NO dissociation constant $K_D \approx 1$ μM while that of *C. vinosum* Cyt c' (*21*) is ≈0.1 μM. The positively charged Arg-127 side chain contributed to the redox stabilization of the Cyt c' in the NO-binding ferrous form. EPR study of whole cells has provided evidence of detectable NO-Cyt c' within *R. sphaeroides* cells (*4*), and that would imply that the internal concentration of NO within cells is on the order of 1 μM. On the other hand, the K_m of the subsequent denitrifying enzyme NO reductase, which converts NO to N_2O, has been estimated to be in the nanomolar range (*29*, *30*), so that denitrifying cells might be expected to have an internal NO concentration considerably lower than 1 μM. The consensus function of Cyt c' is that it stores and transports metabolic NO (*4*, *21*) while protecting against NO toxicity (*31*), and for *R. sphaeroides* and *C. vinosum* Cyts c' (*21*) it should perform these functions at NO concentrations in the 0.1−1.0 μM range.

SUPPORTING INFORMATION AVAILABLE

Cytochrome c' mutagenesis and expression, materials for mutagenesis, and methods of expression and purification; Figure 1S, SDS−PAGE gel electrophoresis of wild type and R127A mutants; Figure 2S, UV−vis absorption spectra NO-bound Cyt c' from wild type and R127A; Figure 3S, comparison of first derivative Q-band EPR spectra of NO-ligated wild type and R127A; Figure 4S, figure showing the similarity of ferric heme EPR spectra from wild type and R127A; Figure 5S, figure showing the similarity of heme and histidine ENDOR features from the ferric heme center of wild type and R127A; Figure 6S, NO titration curves complementary to those in Figure 8 for R127A and wild-type Cyt c'; Figure 7S, a plot of the ratio NO-bound to NO-unbound heme as a function of NO concentration for R127A and wild-type Cyt c'. This material is available free of charge via the Internet at http://pubs.acs.org.

REFERENCES

1. Lawson, D. M., Stevenson, C. E., Andrew, C. R., and Eady, R. R. (2000) Unprecedented proximal binding of nitric oxide to heme: implications for guanylate cyclase. *EMBO J. 19*, 5661–5671.
2. Lawson, D. M., Stevenson, C. E., Andrew, C. R., George, S. J., and Eady, R. R. (2003) A two-faced molecule offers NO explanation: the proximal binding of nitric oxide to haem. *Biochem. Soc. Trans. 31*, 553–557.
3. Ramirez, L. M., Axelrod, H. L., Herron, S. R., Rupp, B., Allen, J. P., and Kantardjieff, K. A. (2003) High resolution crystal structure of ferricytochrome c' from *Rhodobacter sphaeroides*. *J. Chem. Crystallogr. 33*, 413–424.
4. Choi, P. S., Grigoryants, V. M., Abruna, H. D., Scholes, C. P., and Shapleigh, J. P. (2005) Regulation and function of cytochrome c' in *Rhodobacter sphaeroides* 2.4.3. *J. Bacteriol. 187*, 4077–4085.
5. Choi, P. S.-T. (2004) Ph.D. Thesis, Department of Microbiology, Cornell University, Ithaca, NY.
6. Usov, O. M., Choi, P. S.-T., Shapleigh, J. P., and Scholes, C. P. (2005) ENDOR investigation of the liganding environment of mixed-spin ferric cytochrome c'. *J. Am. Chem. Soc. 127*, 9485–9494.
7. Marti, M. A., Capece, L., Crespo, A., Doctorovich, F., and Estrin, D. A. (2005) Nitric oxide interaction with cytochrome c' and its relevance to guanylate cyclase. Why does the iron-histidine break? *J. Am. Chem. Soc. 127*, 7721–7728.
8. Usov, O. M., Choi, P. S., Shapleigh, J. P., and Scholes, C. P. (2006) ENDOR of NO-ligated cytochrome c'. *J. Am. Chem. Soc. 128*, 5021–5032.
9. Hayes, R. G., Ellison, M. K., and Scheidt, W. R. (2000) Definitive assignment of the g tensor of [Fe(OEP)(NO)] by single-crystal EPR. *Inorg. Chem. 39*, 3665–3668.
10. Barbieri, S., Murphy, L. M., Sawers, R. G., Eady, R. R., and Hasnain, S. S. (2008) Modulation of NO binding to cytochrome c' by distal and proximal haem pocket residues. *J. Biol. Inorg. Chem. 13*, 531–540.
11. Thöny-Meyer, L. (1997) Biogenesis of respiratory cytochromes in bacteria. *Microbiol. Mol. Biol. Rev. 61*, 337–376.
12. Sienkiewicz, A., Smith, B. G., Veselov, A., and Scholes, C. P. (1996) Tunable Q-band resonator for low temperature electron paramagnetic resonance/electron nuclear double resonance measurements. *Rev. Sci. Instrum. 67*, 2134–2138.
13. Usov, O. M., Sun, Y., Grigoryants, V. M., Shapleigh, J. P., and Scholes, C. P. (2006) EPR-ENDOR of the Cu(I)NO complex of nitrite reductase. *J. Am. Chem. Soc. 128*, 13102–13111.
14. Reinhammar, B. R. M. (1972) *Biochim. Biophys. Acta 275*, 245–249.
15. O'Reilly, J. (1973) Oxidation-reduction potential of the ferro-ferric-cyanide system in buffer solutions. *Biochim. Biophys. Acta 292*, 509–515.
16. Hoffman, B. M., DeRose, V. J., Doan, P. E., Gurbiel, R. J., Houseman, A. L. P., and Telser, J. (1993) in Biological Magnetic Resonance, Vol. 13: EMR of Paramagnetic Molecules (Berliner, L. J., and Reuben, J., Eds.) Plenum, New York.
17. Andrew, C. R., Green, E. L., Lawson, D. M., and Eady, R. R. (2001) Resonance Raman studies of cytochrome c' support the binding of NO and CO to opposite sides of the heme: implications for ligand discrimination in heme-based sensors. *Biochemistry 40*, 4115–4122.
18. Cusanovich, M., Tedro, S. M., and TitanKamen, M. D. (1970) *Pseudomonas denitrificans* cytochrome cc'. *Arch. Biochem. Biophys. 141*, 557–570.
19. Derbyshire, E. R., Gunn, A., Ibrahim, M., Spiro, T. G., Britt, R. D., and Marletta, M. A. (2008) Characterization of two different five-coordinate soluble guanylate cyclase ferrous-nitrosyl complexes. *Biochemistry 47*, 3892–3899.
20. Romberg (1982) Ph.D. Thesis, Department of Chemistry, University of Illinois at Chicago, Chicago, IL.
21. Mayburd, A. L., and Kassner, R. J. (2002) Mechanism and biological role of nitric oxide binding to cytochrome *c'*. *Biochemistry 41*, 11582–11591.
22. Zhang, Y., Gossman, W., and Oldfield, E. (2003) A density functional theory investigation of Fe-N-O bonding in heme proteins and model systems. *J. Am. Chem. Soc. 125*, 16387–16396.
23. Fujisawa, K., Tateda, A., Miyashita, Y., Okamoto, K., Paulat, F., Praneeth, V. K., Merkle, A., and Lehnert, N. (2008) Structural and spectroscopic characterization of mononuclear copper(I) nitrosyl complexes: end-on versus side-on coordination of NO to copper(I). *J. Am. Chem. Soc. 130*, 1205–1213.
24. Scheidt, W. R., and Ellison, M. K. (1999) The synthetic and structural chemistry of heme derivatives with nitric oxide ligands. *Acc. Chem. Res. 32*, 350–359.
25. Andrew, C. R., George, S. J., Lawson, D. M., and Eady, R. R. (2002) Six- to five-coordinate heme-nitrosyl conversion in cytochrome c' and its relevance to guanylate cyclase. *Biochemistry 41*, 2353–2360.
26. George, S. J., Andrew, C. R., Lawson, D. M., Thorneley, R. N., and Eady, R. R. (2001) Stopped-flow infrared spectroscopy reveals a six-coordinate intermediate in the formation of the proximally bound five-coordinate NO adduct of cytochrome c'. *J. Am. Chem. Soc. 123*, 9683–9684.
27. Pixton, D. A., Petersen, C. A., Franke, A., van Eldik, R., Garton, E. M., and Andrew, C. R. (2009) Activation parameters for heme-NO binding in *Alcaligenes xylosoxidans* cytochrome c': the putative dinitrosyl intermediate forms via a dissociative mechanism. *J. Am. Chem. Soc. 131*, 4846–4853.
28. Moore, G. R., and Pettigrew, G. W. (1990) Cytochromes c: Evolutionary, Structural, and Physicochemical Aspects , Springer-Verlag, Berlin.
29. Goretski, J., and Hollocher, T. C. (1990) The kinetic and isotopic competence of nitric oxide as an intermediate in denitrification. *J. Biol. Chem. 265*, 889–895.
30. Goretski, J., Zafiriou, O. C., and Hollocher, T. C. (1990) Steady-state nitric oxide concentrations during denitrification. *J. Biol. Chem. 265*, 11535–11538.
31. Cross, R., Aish, J., Paston, S. J., Poole, R. K., and Moir, J. W. (2000) Cytochrome c' from *Rhodobacter capsulatus* confers increased resistance to nitric oxide. *J. Bacteriol. 182*, 1442–1447.